

Direct Recycling of Cold Work Tool Steel Swarf into New Cutting Disks via Field-Assisted Sintering

Monica Keszler,* Felix Großwendt, Olivier Guillon, Sebastian Weber, and Martin Bram

Grinding swarf on the micrometer scale is produced when steel tools are machined to their final shape. The morphology of this swarf is prone to trapping lubricant and grinding medium, such as Al_2O_3 and SiC . Due to both shape and contamination, the swarf is considered undesirable for direct recycling. However, utilizing a consolidation technique, such as field-assisted sintering technology/spark plasma sintering (FAST/SPS), a unique composite material can be made from embedding or dissolving ceramic grinding contaminants into the steel matrix. Herein, ceramic-contaminated D2 steel swarf, dried from lubricant, is sintered into a 120 mm diameter cutting disk. This disk is then capable of removing sandstone when tested in a mock tunneling rig. The work explores the challenges in scaling up FAST/SPS sintering from 20 mm test samples up to full scale, the extent of SiC dissolution during sintering, and the optimization of postsintering heat treatment parameters.

million tons of metal are lost through machining. This loss of metals detracts from the available supply of already limited resources. With advances in technology, growth in population, and increasing demand for resources, such a significant disposal of metal scrap leads to the removal of valuable elements from the supply chain that could otherwise be recovered and reused.

Metallic swarf often contains nonmetallic waste products as well, such as grinding medium and lubricant from the machining process. In machining processes such as turning or milling, the metallic waste tends to have a larger particle size, referred to as chips. These metallic chips can be pressed to remove residual cutting fluid before reuse in production.^[3] Recycling of larger

chips can already be observed at the industrial level through various means, such as extrusion.^[4]

Waste consisting of smaller sized metallic particles from processes such as grinding, however, comes with a variety of other challenges before it can be prepared for recycling. Grinding swarf can come in a number of different morphologies depending on the material properties of the metal and on what grinding wheel material it was exposed to.^[5,6] When particles are tendril or spiral-shaped, they are more likely to latch onto one another and form agglomerates. These agglomerates can trap residual cooling lubricant, which was used during the grinding process to dissipate heat and increase grinding efficiency.^[7] They can also trap abrasive particles that dislodged from grinding wheels.

As grinding lubricant and metallic swarf can often be harmful to human health, grinding sludge is often sent directly to landfill, which involves both significant costs and burdens the environment.^[4,8] However, a variety of techniques to clean the swarf from the lubricant have been explored, including combusting the lubricant or separation via supercritical CO_2 extraction.^[9–11] These processes are cost intensive. When combined with the energy needed to re-melt the swarf for further recycling, the whole recycling process is considered to be quite complex and uneconomical. Therefore, grinding sludge recycling has not been implemented on a large scale.^[8]


The push for furthering material recycling continues to grow, though. The steel of interest in this study, a cold work tool steel called AISI D2, includes high Cr, Mo, and V contents, elements of which are increasing in demand for steel production.^[12] This type of steel is useful in cases requiring high wear resistance and non-deforming properties.^[13] In the case of the production of cutting disks from cold work tool steel, mass loss during grinding can

1. Introduction

To develop metallic tools and products into their final desired shapes, dimensional tolerances, and surface finishes, it is often necessary to subject tools to machining, such as through grinding or turning. As machining is a subtractive process, it produces metallic waste. This waste is often referred to as chips or swarf, and they are produced in various sizes and morphologies. Puga et al. have suggested that the total mass loss from machining is roughly 3%–5% the casting weight, in the case of aluminum alone.^[1] In 2019, casting production worldwide was approximated to be roughly 110 million tons across varied metals.^[2] If the 3%–5% weight loss is applied across all metals, then nearly 3–5

M. Keszler, O. Guillon, M. Bram
Materials Synthesis and Processing (IMD-2)
Forschungszentrum Jülich GmbH
Wilhelm-Johnen-Strasse, 52428 Jülich, Germany
E-mail: m.keszler@fz-juelich.de

F. Großwendt, S. Weber, M. Bram
Lehrstuhl Werkstofftechnik
Ruhr-Universität Bochum
Universitätsstraße 150, 44801 Bochum, Germany

 The ORCID identification number(s) for the author(s) of this article can be found under <https://doi.org/10.1002/adem.202501639>.

© 2025 The Author(s). Advanced Engineering Materials published by Wiley-VCH GmbH. This is an open access article under the terms of the Creative Commons Attribution License, which permits use, distribution and reproduction in any medium, provided the original work is properly cited.

DOI: 10.1002/adem.202501639

reach over 50%. For broaching tools, this mass loss is even higher, reaching 60%–70%.^[14] Efforts to avoid landfilling grinding sludge have elevated due to environmental protection regulations, movement toward a circular economy, and the reduction of economical and geopolitical dependencies.^[15–17]

Simplified stages of cleaning D2 sludge, combined with powder metallurgical processing via field-assisted sintering techniques (FAST), are therefore explored as an alternative recycling route in this work. Powder metallurgical techniques display an attractive advantage over re-melting, as the sintering of metals requires much lower temperatures and thus requires less energy.^[18,19] Another added benefit of powder metallurgy is the potential to generate net-shaped parts, reducing the need for machining and minimizing the creation of more swarf.^[20] Though options exist to optimize particle size and morphology of cleaned grinding swarf using a technique such as plasma spheroidizing,^[21] less energy-intensive forms of particle size control, such as ball milling, are capable of producing metal powders suitable for powder metallurgical processes from the swarf.^[22] A variety of powder metallurgical processes have been examined for this type of swarf, including vacuum sintering,^[23] liquid phase sintering,^[23] hot isostatic pressing,^[23] and electric discharge sintering.^[14]

Field-assisted sintering technology/spark plasma sintering (FAST/SPS) is a consolidation technique involving the application of uniaxial pressure and a pulsed current to powder placed within an electrically conductive die. This is done to sinter powder in a significantly reduced amount of time compared to conventional sintering or hot pressing.^[24,25] The die surrounding the powder heats up via Joule heating and thus provides heating from the outside of the powder. Simultaneously, as the powder is conductive, the current passing through heats the swarf internally by Joule heating. As the powder is heated both internally and externally, a high heating rate in the range of several 100 K min^{−1} can be achieved, leading to a high rate of mass transfer and rapid consolidation.^[26] Sintering with FAST/SPS allows for the possibility of mixed materials to be sintered together, leading to a composite with additive particles suspended in a matrix. For example, grinding swarf could form a composite of steel and Al₂O₃.^[27] FAST/SPS has been utilized in the consolidation of a number of different metals, such as titanium,^[26,28,29] aluminum,^[30] and copper,^[31] though industrial scale FAST/SPS processes for many of these materials have not yet been realized. As oxidation of the grinding swarf occurs during the grinding process of a steel tool, due to the swarf reaching temperatures above 1000 °C,^[32] a reducing agent in the form of a powder or gas may be necessary to mitigate the amount of oxides present.^[33] Electric current-assisted sintering processes, like FAST/SPS, have been suggested to be capable of breaking down the oxide layer on metallic particles during the sintering process, which is especially useful in the case of oxidized grinding swarf.^[24,34] FAST/SPS also has the advantage of using significantly less energy than hot pressing, with savings potentially being in the range of 90%–95%.^[35] FAST/SPS has previously been shown to successfully consolidate irregularly shaped powder into fully dense parts, such as with crushed Nd–Fe–B magnet scrap.^[36] The possibility of FAST/SPS processes working with unconventionally shaped powder, combined with its energy-saving potential, makes it an attractive candidate for the direct recycling of steel swarf.

This work focuses on the production of D2 grinding waste into the form of a cutting disk via FAST/SPS sintering for mechanized tunneling. As this D2 grinding waste is recovered from the grinding of circular knives, it is also expected that the waste can be sintered for use again as knives. Using the disks in a mechanized tunneling rig helps in the investigation of other advantages of the recycled material, such as the changes in mechanical performance provided by the embedding of grinding medium like Al₂O₃. A cutting disk was chosen as a simple-to-realize demonstrator part, considering the limited net-shaping capabilities of the FAST/SPS tools available. This study was also performed, more generally, as a proof of concept for the FAST/SPS sintering of other potential steel swarf.

2. Experimental Section

2.1. Considered Grinding Waste

The grinding waste, also referred to as swarf, considered in this study, originates from the production of circular knives. The knives are produced from cold work tool steel type AISI D2 (DIN 1.2379, X153CrMoV12). D2 tool steel exhibits a ledeburitic microstructure consisting of eutectic Cr-rich carbides of type M₇C₃ embedded in tempered martensite.^[37] This microstructure is produced through quenching and tempering. Grinding of the circular knives is performed in a heat-treated condition to reduce warping in various dimensions, which is caused by quenching. Grinding is performed using a water-based lubricant containing 3%–5% of type Syntilo 81 E oil (Castrol, UK) and polymer-bonded grinding wheels containing both Al₂O₃ and SiC. After grinding, the steel chips that are removed from the tool are contaminated with the cooling lubricant and abrasive particles from the grinding wheels. The grinding waste supplied was dried in an air stream at 140 °C for 48 h.

2.2. FAST/SPS-Processing of the Grinding Chips

Initial FAST/SPS parameters were optimized on a lab scale before upscaling to the final 120 mm cutting disks. Therefore, 5 g of D2 grinding swarf was precompacted into a graphite die (SGL Carbon, SIGRAFINE R7710) with an inner diameter of 20 mm. For tool preservation and improvement of sample contact, a graphite foil with thickness 0.38 mm (SGL Carbon, SIGRAFEX) was inserted. FAST/SPS was performed in an HP-D5 device (FCT Systeme GmbH, Rauenstein, Germany) at a variety of temperatures, pressures, and dwell times to densify the steel. Boron nitride spray was applied in a 0.02 mm thick coating on all graphite foil in contact with the steel material. Initial experiments involved graphite foil that was not coated with boron nitride, leading to carbon uptake. Dr. Fritsch Boron-Nitride Spray (Dr. Fritsch GmbH & Co. KG, Fellbach, Germany) was used for this purpose. Ultimately, the chosen parameter set carried over into upscaling is listed in **Table 1**. This parameter set leads to a recylate material density of roughly 7.2 g cm^{−3}, which is 94% of the density of the original D2 steel. It is vital to note that the theoretical density of the recylate is reduced compared to the original steel due to SiC and Al₂O₃ particles included as residues from the grinding process. 120 mm diameter samples were sintered in a Dr. Fritsch DSP515 FAST/SPS device

Table 1. Chosen FAST/SPS parameter for the sintering of small- and large-scale D2 steel disks.

Maximum temperature	950 [°C]
Maximum pressure	45 [MPa]
Dwell time	1 [min] and 5 [min]
Heating rate	100 [K min ⁻¹]
Steel powder mass	5 [g] and 250 [g]
Graphite die diameter	20 [mm] and 120 [mm]
Cooling rate (to 300 [°C])	90 [°C min ⁻¹]
$t_{8/5}$	192 [s]

(Dr. Fritsch GmbH & Co. KG, Fellbach, Germany). For the ease of inserting and removing punches, the circumferential graphite foil was pressed from a thickness of 0.38 to 0.28 mm using a hydraulic press. Boron nitride spray was applied only to the areas of the foil with contact to the steel, as full BN coverage caused too much mechanical resistance to the punches sliding into the die. A schematic of the FAST/SPS set-up used for 120 mm diameter disks is shown in **Figure 1**. 250 g of D2 grinding waste was incrementally placed into the die and regularly smoothed for a consistent height. This mass of powder was chosen to generate a sintered disk of roughly 3 mm in height. Cooling occurred at a rate of 90 °C min⁻¹, with a $t_{8/5}$ of 192 s. The value $t_{8/5}$ is the amount of time it takes for the material to cool from 800 to 500 °C and is considered the most critical cooling range for carbon and low alloy steels. It plays a large role in determining the microstructure of the steel.^[38,39] After sintering and cooling, the samples were extracted with a hydraulic press and cleaned from graphite foil manually with a knife before sandblasting.

2.3. Chemical Analysis

The chemical composition of the grinding chips was measured by X-ray fluorescence analysis (XRF) using a type Niton XL2 air

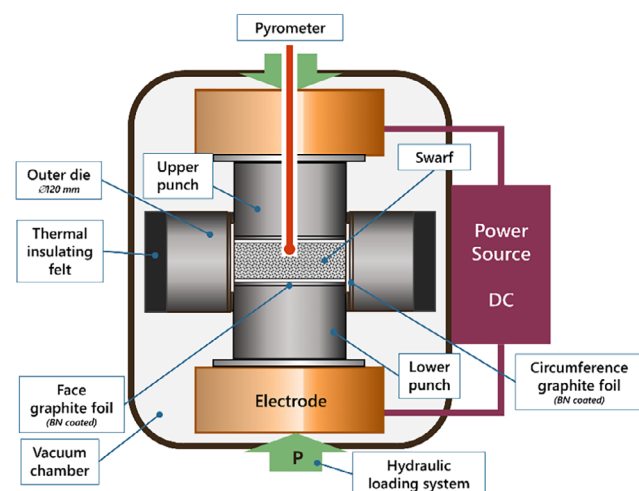


Figure 1. Schematic of the FAST/SPS set-up used for the sintering of 120 mm D2 disks.

by Thermo Scientific (USA). Through this method, only elements heavier than Mg could be quantified. The contents of the light elements C, N, and O were therefore determined by carrier hot gas extraction (CHGE). C analysis was performed using a type CS-800 by Eltra (Germany) while measurement of N and O contents was performed using a type TCH 600 by Leco (USA). 300 to 500 mg of sample mass were analyzed within one measurement. The C, N, and O contents given are the averages of three individual measurements.

2.4. Thermodynamic Calculations

To estimate suitable heat treatment parameters of the FAST/SPS-processed swarf, thermodynamic calculations were performed using the software Thermocalc v. 2024a (Thermocalc AB, Sweden).^[40] Calculations were performed in equilibrium condition based on the database TCFe10.^[41] The considered phases were ferrite, austenite, M₇C₃, M₃C, M₂₃C₆, MC, SiC, MSi, MSi₂, M₃Si, M₅Si₃, and liquid. The O and Al contents of the grinding waste were neglected for the calculations as the Al₂O₃ abrasive particles present within the waste behave inertly.

2.5. Further Processing of the FAST/SPS Samples

As austenitization was expected to occur during the FAST/SPS sintering cycle, the recycle disk was subjected to direct tempering (triple tempering at 540 °C for 2 h). To mount the FAST/SPS-produced on the shaft of a mechanized tunneling test rig, a centered hole of 80 mm was cut by waterjet cutting. **Table 2** gives an overview of all the samples generated, including their variations in graphite foil (C-foil) coatings, dwell times, and thermal treatments.

2.6. Microstructure Characterization

Particle morphology was analyzed via field emission gun scanning electron microscopy (SEM) using a Zeiss Gemini 450 (Carl Zeiss AG, Germany) using an acceleration voltage of 8 kV and working distance of 8.0 mm. A classical Everhardt-Thornley detector was used to image the powder morphology. Micrographs of the sintered samples were taken using a back-scattered electron (BSE) detector to achieve an improved contrast between the individual phases present in the microstructures of the samples. Microstructural analysis was conducted using an SEM type MIRA 3 (Tescan, Czechia) operating at a working distance of 15 mm and an acceleration voltage of 20 kV. The increased acceleration voltage was chosen to enable energy-dispersive X-ray spectroscopy (EDX) measurements with the fitted X-Mas 50 detector (Oxford Instruments, UK). Contents of retained austenite (RA) were measured using X-ray diffraction applying a μ x-360 (Pulsetec, Japan). Full Debye rings from a single incident X-ray angle were collected to be converted to intensity/2 θ -diagrams. According to the Rietveld method, the retained austenite content was calculated. Vickers hardness measurements were conducted using a KB30s system (KB-Prüftechnik, Germany). For hardness, the mean of five individual measurements was calculated.

Table 2. Sample names of D2 pellets FAST/SPS sintered at 950 °C, 45 MPa with variations to dwell time and tempering (tempering conditions are listed in Section 2.5).

Sample name	Protective foil	Sample diameter [mm]	Powder mass [g]	Dwell time [min]	Posttreatment
20 [mm]-1 [min]-C	C-foil	20	5	1	–
20 [mm]-5 [min]-C	C-foil	20	5	1	–
20 [mm]-1 [min]-BN	C-foil + BN	20	5	1	–
20 [mm]-5 [min]-BN	C-foil + BN	20	5	1	–
120 [mm]-1 [min]	C-foil + BN	120	250	1	–
120 [mm]-5 [min]	C-foil + BN	120	250	5	–
120 [mm]-5 [min]-T	C-foil + BN	120	250	5	Tempering

2.7. Tunneling Rig Testing

After shaping and heat treatment, both the D2 swarf disk and a D2 reference disk were tested on a mock tunneling device.^[42] A counterpart of cylindrical sandstone from Anröchte, Germany was used as a tunneling surface. The disks were rotated counter to the cylinder. A static load of 2500 N was applied to the disks which dynamically increased to 5000 N during testing. The tests were run for 20 min. After completion of the tests, the weight of the excavated material and the weight loss of the disk were measured.

3. Results and Discussion

3.1. Cleaning Procedure and Properties of the Grinding Chips

The morphology of the grinding swarf was tendril and spiral-shaped, which is responsible for the ease of trapping grinding medium, such as Al_2O_3 , as seen in **Figure 2A**. A grinding particle is seen as the dark grey shape contained within the light grey steel. The interlocking spirals, as seen in **Figure 2B**, also trap air. This results in the poor bulk and tap density of 0.84 ± 0.03 and $1.39 \pm 0.01 \text{ g cm}^{-3}$, respectively. The poor bulk and tap density thus make this powder non-ideal for traditional powder metallurgical techniques. Both Hall and Carney flow tests could not be performed successfully because of agglomerates blocking the opening of the funnel. Unlike in the work by Großwendt et al., this swarf was not subjected to any form of magnetic separation,

and the only cleaning it experienced from its water-based lubricant was drying in a stream of hot air (48 h at 140 °C).^[14]

Table 3 shows the chemical composition of D2 according to ASTM A681, compared to the chemical analysis of the dried D2 swarf. The comparison between the two reveals an increased C content in the recycle swarf, compared to that of ASTM A681 D2 steel. This can be primarily attributed to SiC contamination, as the Si content is also drastically higher in the swarf than in the standard D2 steel. Organic residuals like oils from the water-based cutting emulsion could have contaminated the particle surfaces as well, resulting in a further increased total carbon content of the swarf. It is expected that residual oil will evaporate prior to the FAST/SPS sintering as the swarf is exposed to a vacuum prior to the application of an electrical field. In addition, the presence of aluminum and increased oxygen contents is observed within the swarf. As a reference, commercially gas-atomized steel powder has been reported in literature to contain less than 150 ppm of oxygen (0.015 mass%).^[43] The high oxygen content in the swarf can be attributed to two aspects: first, the high oxygen content, as well as the high aluminum content, can be traced back to the presence of Al_2O_3 abrasive particles. Second, increased measured oxygen contents could be attributed to the oxidation of the particle surfaces, likely due to the grinding process and the subsequent cleaning procedure.

3.2. Small-Scale FAST/SPS Testing

In a previous work by Keszler et al., various FAST/SPS dwell times were tested on 20 mm, 5 g samples to determine the effect

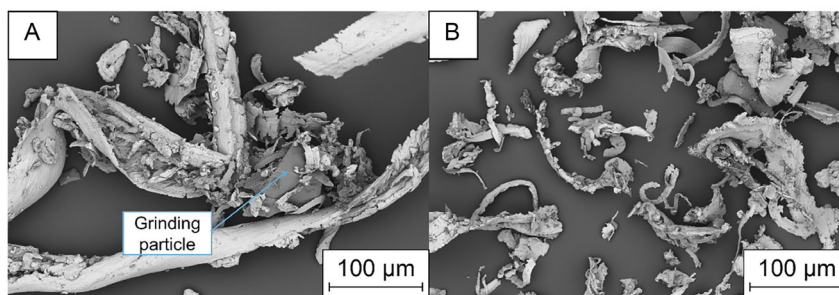


Figure 2. SEM images of the D2 powder, showing A) a grinding particle (labeled) trapped within the spiral-shaped powder and B) the general spiral shape of the powder.

Table 3. Chemical composition of AISI D2 steel from ASTM A681 compared to the swarf in mass%. All elements in the swarf determined by XRF *(C, N, and O were measured by CHGE).

	C*	Si	Mn	Cr	Mo	V	Al	O*	N*	Fe
ASTM A681	1.4–1.6	0.1–0.6	0.1–0.6	11–13	0.7–1.2	0.5–1.1	–	–	–	Bal.
D2 swarf	3.19 ± 0.03	3.92 ± 0.59	0.41 ± 0.01	10.90 ± 0.05	0.68 ± 0.01	0.72 ± 0.03	2.90 ± 0.06	0.884 ± 0.068	0.11	Bal.

of dwell time on RA content and density.^[44] These experiments were repeated for this work. A key component of this FAST/SPS sintering was the application of boron nitride spray as a barrier between the D2 steel swarf and the C-foil used to protect the graphite tools during the sintering process. As seen in **Table 4**, the use of a BN coating significantly mitigated the diffusion of carbon into the D2 steel from the C-foil. Therefore, all subsequent experiments involving the FAST/SPS sintering of D2 used a BN coating between the steel powder and the C-foil to control carbon diffusion. Also of note is that C-content is lower in the samples sintered with BN as opposed to the starting powder (see **Table 3**). This is a sign that lubricant oil was left behind, or that other organics, such as disinfectants or binders from the grinding, are evaporating due to the vacuum and heat applied during the FAST/SPS process. It is expected that the carbon content of 2.47 mass% within the samples sintered by FAST/SPS while using the BN-coated foil reflects solely the contamination with SiC abrasive particles and minor remnants of the polymer binder of the grinding wheels.

Based on the work by Keszler et al., the two shortest sintering dwell times of 1 min and 5 min were repeated. This was due to the results finding no significant difference between the sintering times and the final sample density, as seen in **Table 5**. Lowering sintering times leads to better energy savings, which is favorable from both economic and ecological standpoints. This led to the choice of sintering larger-scale disks with a 1 min dwell time, as the small-scale samples suggested there would be no improvement from an increase of dwell time.^[44]

3.3. FAST/SPS of D2 into 120 mm Disks and Subsequent Heat Treatment

Table 6 shows the measured Archimedes densities of the 20 mm diameter and 120 mm diameter samples. As it was seen that there was a large discrepancy between the 1 min dwell FAST/SPS samples of 20 mm diameter and 120 mm diameter, the possibility to directly transfer the FAST/SPS parameters successfully used for laboratory scale 20 mm sample to the upscaled 120 mm samples was questioned. Due to limitations of the Dr. Fritsch

Table 4. Global C contents of the samples sintered with varying process parameters in mass% measured by CHGE.

Sample name	C content in mass%
20 [mm]-1 [min]-C	2.57 ± 0.02
20 [mm]-1 [min]-BN	2.44 ± 0.00
20 [mm]-5 [min]-C	3.53 ± 0.02
20 [mm]-5 [min]-BN	2.47 ± 0.02

Table 5. Density measurements of 20 mm sintered D2 samples with 1 and 5 min dwell times.

Sample name	Measured density in g cm ⁻³ [44]
20 [mm]-1 [min]-BN	7.19 ± 0.01
20 [mm]-5 [min]-BN	7.20 ± 0.01

Table 6. Measured density for sintered D2 disks of varied sintering parameters.

Sample	Measured density in [g cm ⁻³]
20 [mm]-1 [min]-BN	7.19 ± 0.01
120 [mm]-1 [min]	6.57 ± 0.05
20 [mm]-5 [min]-BN	7.20 ± 0.01
120 [mm]-5 [min]	7.11 ± 0.03

DSP515, increasing pressure was not a possibility. As the powder mass was increased from 5 to 250 g in scale-up, with no other major changes in processing parameters, it was thought that the center of the larger sample would not experience the same increase in temperature as the smaller sample. With a longer dwell time, the chance increased to have a more homogeneous and steady temperature distribution for a longer period of time. A dwell time of 5 min was chosen as, though it is five times greater than the 1 min dwell, it only increases total processing time by 4 min. Increased dwell time was also thought to bring other benefits to the sample processing. Any organic matter that was left behind from the lubricant would have a longer time to be cracked and either diffuse into the steel or outgas into the FAST/SPS vacuum. SiC contaminants would have a longer opportunity to dissolve during the FAST/SPS stage.

As mentioned before, both 20 mm-1 min-BN and 20 mm-5 min-BN exhibited a density of roughly 7.2 g cm⁻³. The different sintering times of 1 and 5 min did not appear to alter the level of densification significantly. Considering that the sintered recycle material is a composite material consisting of D2 steel admixed with 5.1% Al₂O₃ and 4.7% SiC particles, the measured density of the 20 mm samples equals 98.6% of the theoretical density of the composite. These small-scale samples initially hinted that 1 min sintering time at 950 °C is sufficient at the given pressure to fully densify the recycle material. However, for the reasons mentioned above, the 120 mm samples did not reflect an equivalent density when sintered with a 1 min dwell time during FAST/SPS. 120 mm-5 min increased in density nearly 8% relative to 120 mm-1 min, leading to a relative density of roughly 97.4%.

This discrepancy can be seen in the SEM images in **Figure 3A** and B, with the 1-min dwell sample displaying larger pores than the 5 min dwell sample. The density achieved after applying the 5 min dwell time during FAST/SPS was considered high enough to focus only on an adapted postsintering hardening for 120 mm-5 min. Still, the densification was not perfect, as can be seen in **Figure 3B**, which shows the as-sintered sample still containing pores. Oxides on the former surfaces of the grinding chips can be seen in dark grey. Despite the imperfections, the micrograph of 120 mm-5 min shows clear improvement over 120 mm-1 min.

As energy consumption data were not collected for 120 mm-5 min, estimates were made based on the energy consumption of the 120 mm-1 min cycle. As seen in **Figure 4A**, the application of force, temperature increase, and plunge displacement is displayed. Energy consumption during dwell is estimated to be

roughly 15 Wh s^{-1} when a linear fit is applied to the power consumption of the DSP515, as shown in **Figure 4B**. When comparing **Figure 4A** and B, it is clear that only a small energy input is necessary for the application of uniaxial pressure, with the majority of the energy going toward heating. The additional 240 s of dwell would therefore lead to an additional 3.6 kWh of energy consumed by the DSP515 device. The cooler consumes roughly 3 Wh s^{-1} through the sintering cycle, leading to an additional 0.7 kWh of power consumption from the cooler, when the sintering cycle consists of a 5 min dwell. In total, a sintering cycle with a 5 min dwell time should have an energy consumption of roughly 16.8 kWh.

To ensure sufficient toughness and hardness of the steel matrix, the FAST/SPS disks were subjected to a direct tempering in the secondary hardness regime. It was initially assumed that

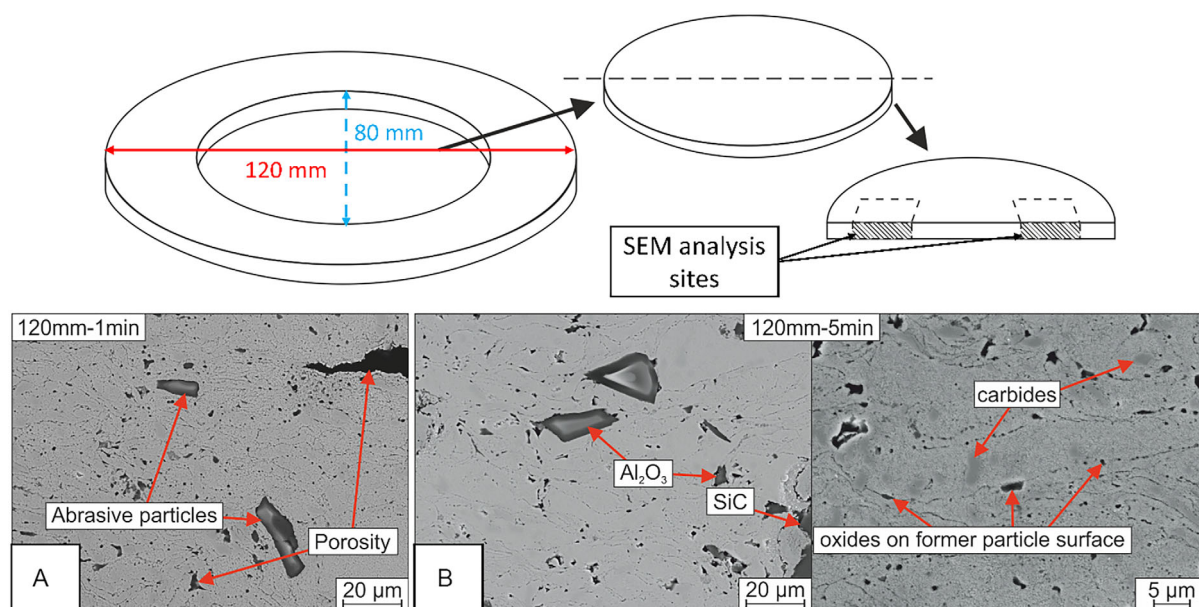


Figure 3. (top) Diagram showing where SEM images were taken from all disks, shown with shading and (bottom) micrographs of the A) 1 min and B) 5 min dwell FAST/SPS sintered sample.

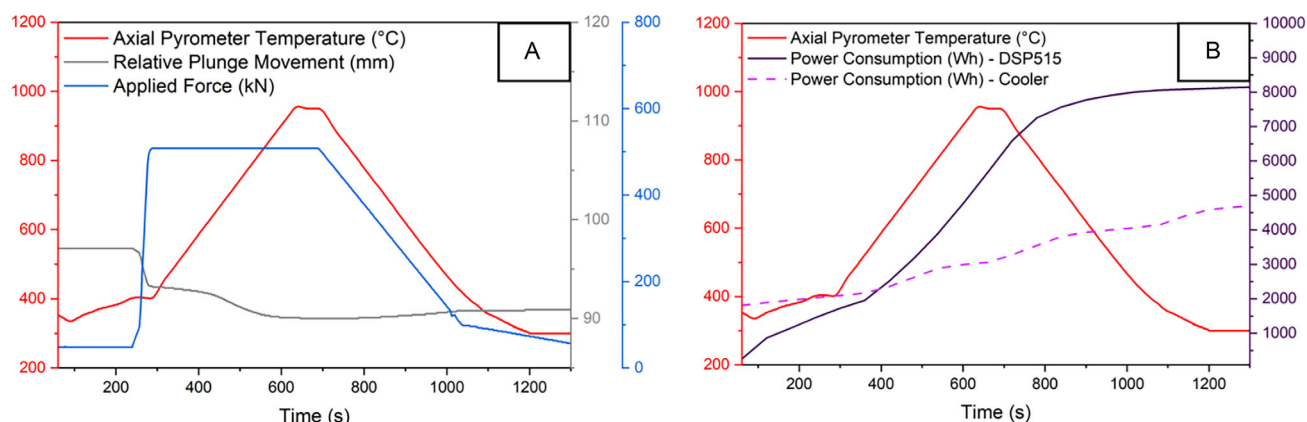


Figure 4. A) Temperature, pressure, and plunge movement data gathered by Dr. Fritsch DSP515 over the course of 120 mm-1 min sintering cycle, B) power consumption of both the Dr. Fritsch DSP515 device and attached cooling device shown relative to the change in temperature over the course of the FAST/SPS sintering cycle.

all SiC ceramic contaminants in the D2 swarf would fully dissolve during FAST/SPS sintering. Therefore, due to the presence of Si and excess C, heat-treatment parameters commonly used for D2 steel could not be directly applied. It was assumed that the increased C content, combined with the cooling rate at the end of the FAST/SPS cycle and $t_{8/5}$ of 192 s, provided a sufficient solution state of C to allow for direct tempering in the secondary hardness regime. Moscoso et al. were able to achieve a hardness of more than 650 HV in D2, when the steel was quenched with a $t_{8/5}$ of up to 280 s, prior to tempering.^[45]

Figure 5A shows thermodynamic calculations for uncontaminated D2 steel, while Figure 5B considers the scenario in which all SiC contaminants in the contaminated D2 swarf have been dissolved into the D2 matrix. Under the assumption that all the SiC would dissolve, the recycle material would contain drastically different solute C content in the austenite phase when compared to pristine D2, at given temperatures. This means that austenitizing temperatures must be reduced for the D2 swarf to prevent excessive amounts of RA. However, due to the Si introduced by SiC in the D2 swarf, the austenite phase region is restricted compared to the D2 reference material. According to the calculation, an austenitizing temperature of more than 960 °C is required to transform all ferrite to austenite in the recycle D2. Higher amounts of M_7C_3 (Cr-carbide) and MC (V-carbide) appear for the recycle due to the higher C-content contributed by SiC. Melt formation also begins at lower temperatures compared to the reference material.

Figure 5 also shows the calculation of stable phases in both reference D2 steel and the recycle D2 steel samples sintered with BN spray. According to Figure 5B, the applied FAST/SPS temperature of 950 °C leads to a calculated volume fraction of remaining

ferrite of 11 vol% and a solute C-content in the formed austenite of 0.6 mass%, which was the target solute C content. This is in accordance with the solute C content in the D2 reference material at the typical austenitizing temperature of 1080 °C, which is also 0.6 mass%. This 0.6 mass% of solute C would ideally lead to an optimum martensite hardness. Unfortunately, the remaining 11 vol% of ferrite left in the recycle D2, which remains from performing FAST/SPS at a temperature of 950 °C, will not be transformed into martensite during cool down or quenching. According to the thermodynamic calculations, based on the compositional make-up of the recycle disk, the D2 recycle should be exposed to an austenitization temperature of more than 960 °C to transform all ferrite into austenite. This, however, would lead to a C-content in the austenite exceeding 0.6 mass%. It needs to be noted that this calculation only considers the complete dissolution of SiC. The partial dissolution of SiC produced solute C and Si contents in-between that of pure D2 steel and of D2 recycle with fully dissolved SiC.

The incomplete dissolution of SiC during the performed sintering can be seen in Figure 6. Contaminants of both SiC and Al_2O_3 can be observed, indicated clearly by the plateaus of Si and Al in the EDX measurement. At the base of the Si plateau, small growths of Si are seen, demonstrating that Si has begun to dissolve into the D2 matrix after FAST/SPS processing. In contrast, the Al_2O_3 appears inert, which was expected. This analysis shows that the considered processing does not completely dissolve the SiC into the matrix but leads to its partial dissolution. The success of SiC dissolution is highly variant based on the size of the SiC particle, and more complete dissolution can occur if the SiC particle is small enough. In Figure 6, a small SiC particle appears to have fully dissolved into the D2 matrix. This led to a

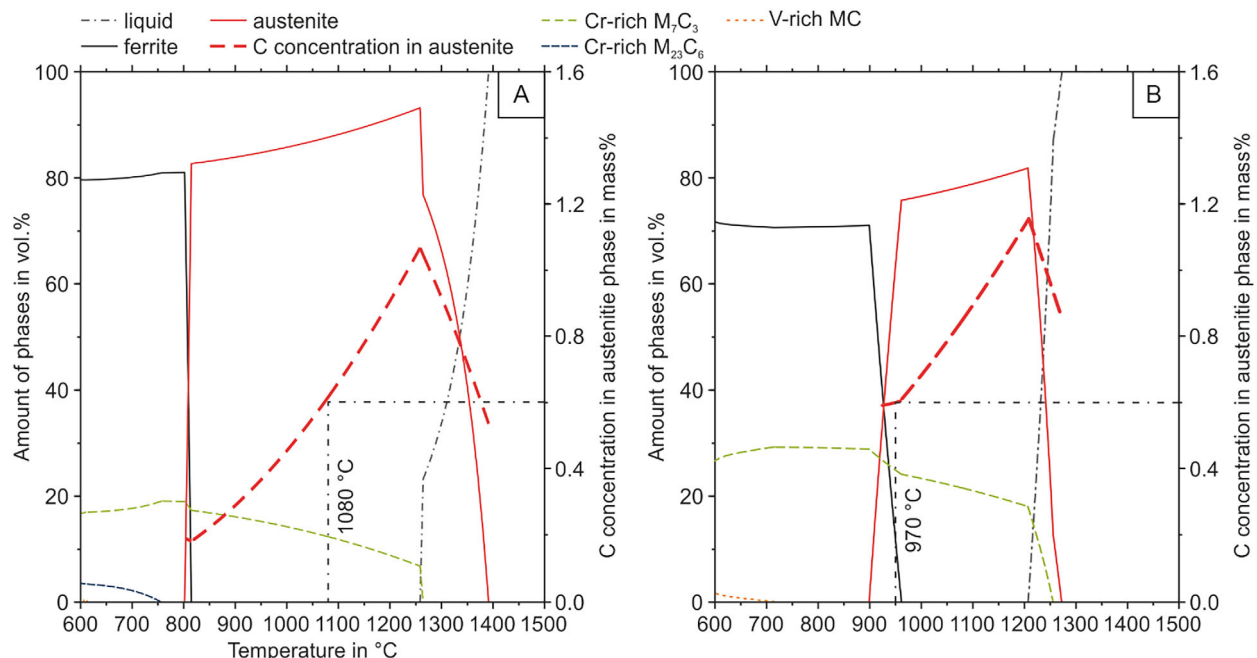


Figure 5. Calculated amounts of stable phases and C concentrations in austenite of A) D2 steel and B) the D2 recycle sintered for 5 min with BN protective coating applied. The black dashed lines represent the abbreviated optimum austenitizing temperatures for both compositions that lead to a solute C content of 0.6 mass%.

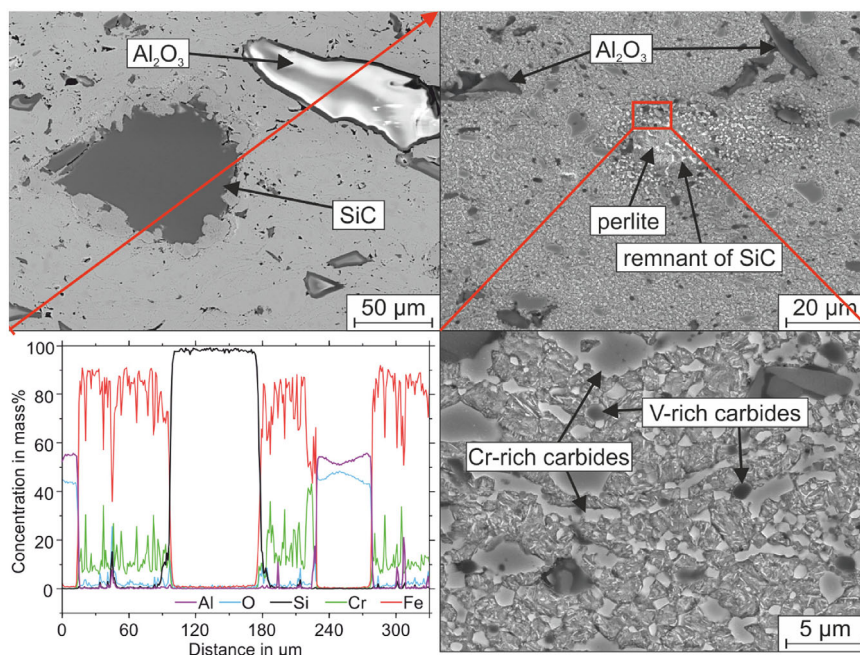


Figure 6. (left) Micrographs of the samples sintered for 5 min in as-FAST condition including an EDX line scan (red line on SEM image), (right) micrographs of 120 mm-5 min-T showing the near full dissolution of a SiC particle into the steel matrix followed by a reprecipitation of finely distributed secondary carbides.

rich collection of carbides, along with the formation of some martensite and pearlite. The wide variation of SiC response and the fact the actual percentage of SiC varies from batch to batch of the grinding waste means that optimal heat treatment is difficult to predict.

With evidence that the SiC would not fully dissolve after FAST/SPS, a heat treatment study was performed to determine what posttreatment could work best for the FAST/SPS D2 swarf disks. Three different heat treatment strategies are considered. One sample was tempered directly after FAST/SPS (FAST/SPS at 950 °C). This sample is labeled as DT. Further austenitization and quenching were done in accordance with the calculations of Figure 5A and B. The calculation shown in Figure 5B which assumes a full dissolution of SiC during FAST/SPS suggests an austenitizing temperature of 970 °C to achieve the desired solute C content of 0.6 mass%. The sample austenitized at 970 °C is labeled “low” in Figure 7, as it is a lower austenitization temperature than what is traditionally used for D2. Additionally, a third sample was austenitized at 1080 °C, which corresponds to a more standard austenitization temperature for D2. This temperature leads to a solute C-content of 0.6 mass% if nearly none of the contaminating SiC is dissolved into the steel matrix (Figure 5A). This third sample is labeled “high” in Figure 7, as this refers to the higher austenitization temperature. Figure 7 compares the results of this heat treatment study with low and high austenitization temperatures. Directly after FAST/SPS, the recycled D2 has a hardness over 700 HV30.

Tempering at 540 °C decreases the hardness to 530 HV30, while the same RA content is apparent in the quenched and tempered reference material. Additional austenitizing at the low austenitizing temperature of 970 °C after FAST/SPS processing leads

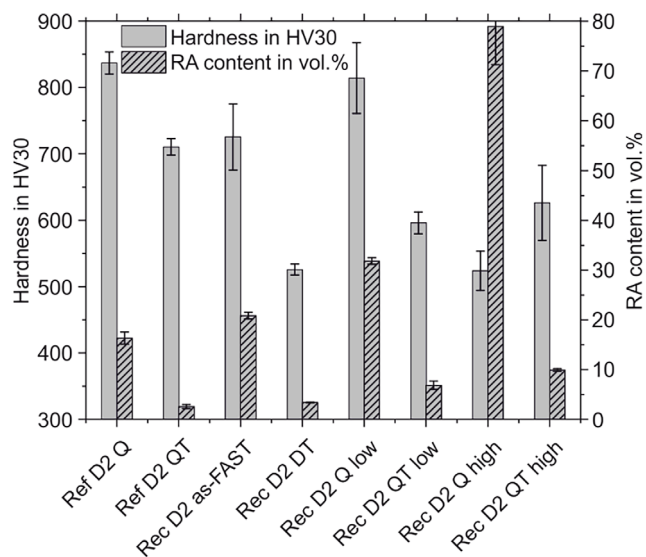


Figure 7. Hardness and RA content of reference D2 and recycled D2 swarf after various heat treatments.

to an initial hardness of more than 800 HV30 which is similar to the hardness of the reference material after quenching. However, a higher RA content is observed. After tempering, the hardness drops to 600 HV30, which is 100 HV30 lower than that of the reference material in application-ready condition. The high temperature austenitizing at 1080 °C generates the highest amount of RA of more than 75%. Consequently, the hardness in quenched condition is reduced to 530 HV30. Tempering increases the hardness

again, leading to a hardness of 640 HV30, which is still 60 HV30 below the hardness of the reference material. This discrepancy in hardness is caused by both the near-dense microstructure and the remaining increased RA content of more than 10%.

No treatment considered here is capable of achieving the target secondary hardness of 700 HV30 which is provided by the D2 reference material, and all options lead to higher RA content than standard D2 as well. Within the scope of the project, the goal was to utilize FAST/SPS as both a consolidation technique and as an austenitizing step. This study made clear that the FAST/SPS parameters, which consisted of a sintering temperature of 950 °C, did not succeed in full austenitization due to insufficient dissolution of SiC. The results of the heat-treatment study suggest an austenitizing temperature that is just slightly reduced compared to the typical austenitizing temperature of 1080 °C, if the samples are austenitized for 20 min. In case of the shorter dwell time at the chosen maximum FAST/SPS sintering temperature, which allows even less dissolution of SiC, future trials should include sintering temperatures of up to 1080 °C to allow successful direct tempering. Nonetheless, the cutting disk that is subjected to further testing in this work is directly tempered after the FAST/SPS processing at 950 °C.

3.4. Testing of the D2 Swarf Disk in Simulated Mechanized Tunneling

The expectation of this work was that the D2 matrix would synergize with the inert Al_2O_3 to generate a metal matrix composite

(MMC) of higher hardness and wear resistance than standard D2. This concept has been explored before by Eifert et al.^[46] Due to the unpredictability of SiC dissolution, though, optimal heat treatment standards could not be developed in this work, and the hardness of standard D2 could not be achieved. Regardless, as seen in **Figure 8A**, the cutting disk made from 120 mm-5 min-T was still able to be installed into the test tunneling rig and to successfully excavate sandstone.^[42] **Figure 8B** and **C** show the two disks before and after tunneling testing, displaying the visible damage on the 120 mm-5 min-T disk. **Table 7** shows an overview of how much sandstone was removed by both the D2 reference disk and the 120 mm-5 min-T disk.

While the disk made from the D2 swarf had a lower hardness than standard D2, it was still able to remove a higher amount of sandstone in the same amount of time when compared to the D2 reference. This could be due to several reasons. First, the 120 mm-5 min-T disk experienced somewhat of a “self-sharpening” effect. This is in reference to pieces breaking off of the disk edge, narrowing the contact area between the disk and the sandstone. As the same amount of force was being applied, the decrease in contact area led to an increase in pressure, causing more sandstone to be removed. Second, pieces of grinding medium, such as Al_2O_3 , were trapped at the edge of the disk as well, as seen in the SEM image in **Figure 9**. The frequency of these particles appearing across the edge of the disk is unknown and their contribution can only be speculated. However, because of their hardness, it is possible that these inclusions assisted somewhat in the abrasion of the sandstone.

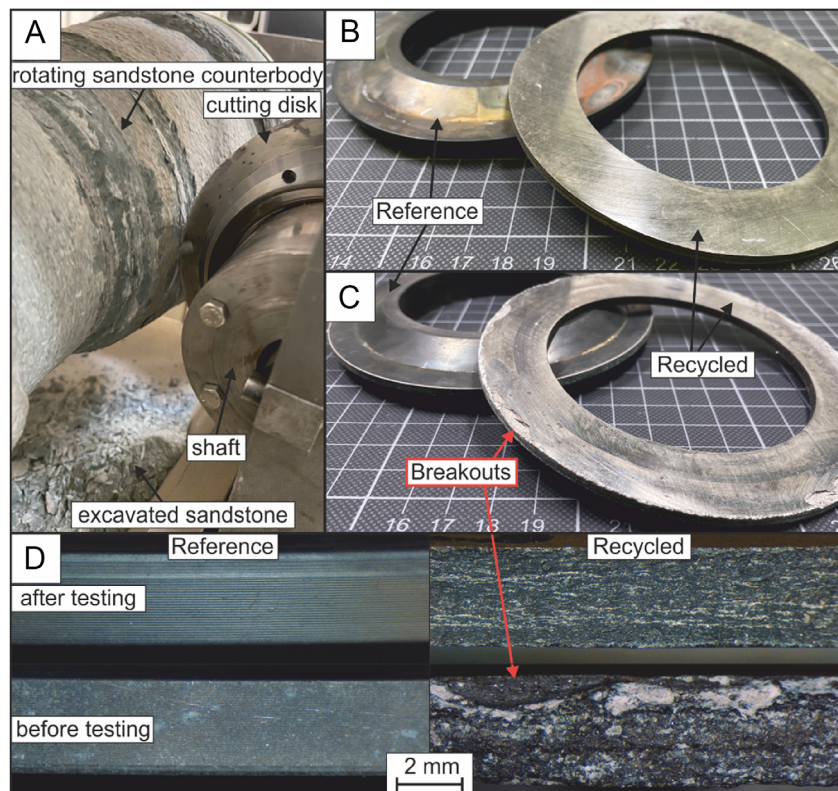


Figure 8. A) Cutting disk produced from D2 grinding waste by FAST/SPS applied in the test rig for mechanized tunneling, and the D2 reference disk compared to the recycled disk B) before and C) after tunneling, and D) optical micrographs of the edges of the disks before and after testing.

Table 7. Mass of sandstone removed and mass of disk lost during tunneling trials for D2 reference and 120 mm-5 min-T disks.

Sample name	Sandstone mass removed [g]	Disk mass lost [g]
D2 reference	78.5	0.0
120 [mm]-5 [min]-T	157.6	2.2

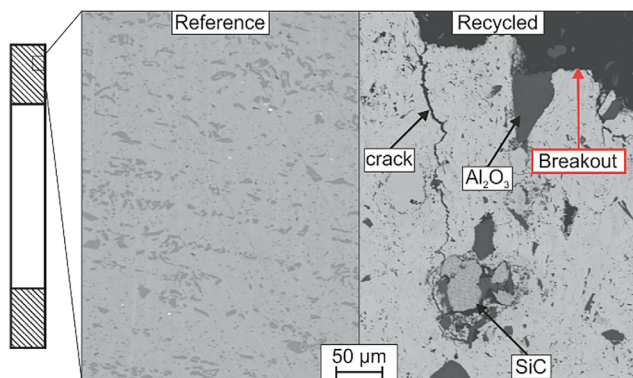


Figure 9. BSE SEM images of the edges of the reference disk and recycled disk after tunneling tests.

While the “self-sharpening” effect of the recycled disk may be beneficial in the short term, long-term usage will mean frequent replacement of the disks. Figure 9 compares the edges of the D2 reference disk with the recycled disk to show the extent of the damage. One notable aspect of the cracking seen in the 120 mm-5 min-T disk is that, in this case, the major cracking is not initiated by the presence of the Al_2O_3 inclusion. Rather, the crack is more likely to follow regions of low density and high oxide concentrations. Due to the geometry of the disk, the pressing direction used during FAST/SPS is perpendicular to the direction of loading during the excavation. The pressing during FAST/SPS, therefore, causes the steel chips to align parallel to the direction of the load forming lines of oxides and volumetric defects that a crack can easily follow. In contrast, the lines of carbides present in the hot-formed D2 reference material are oriented perpendicular to the loading direction which instead can cause deflection of a crack growing from the cutting edge into the material.^[42] The crack observed in Figure 9 terminates at a partly dissolved SiC particle that caused the formation of variety of phases. For more comprehensive conclusions, cyclic compression or impact testing would be necessary.

4. Conclusion and Outlook

A prototype cutting disk was successfully generated from industrial D2 grinding swarf contaminated with grinding lubricant, Al_2O_3 , and SiC from the grinding process. Densification was achieved with FAST/SPS using a maximum temperature of 950 °C, a pressure of 45 MPa, and a dwell time of 5 min. Triple tempering at 540 °C in the regime of secondary hardness transformed excessive retained austenite. However, the target secondary hardness of about 700 HV30 could not be achieved, with final

sample hardness being 535 HV30 after direct tempering subsequent to FAST/SPS. This could be due to residual ferrite in the matrix after heat treatment, which causes the matrix to be unable to sufficiently support the hard phase of Al_2O_3 as it is too soft. If the amount of martensite would be higher, it could be possible that the MMC could achieve a hardness higher than that of D2 alone. Ideally, full austenitization could be performed in the FAST/SPS, but current thermodynamic calculations failed to achieve ideal FAST/SPS temperature as the parameters necessary for fully controlled SiC dissolution during the process are unknown. Regardless, the disk was still capable of withstanding application in a tunneling simulation, and it successfully removed more sandstone than its standard D2 counterpart under the same testing parameters. It exhibited a “self-sharpening” behavior, which increased its pressure on the sandstone in exchange for mass loss during testing.

The thermodynamic calculations suggest exploring a higher FAST/SPS maximum temperature, in the range between 960 and 1080 °C, as this will lead to full austenitization even if no SiC is dissolved during the sintering. Another recommendation would be the removal of SiC entirely, whether through magnetic separation or avoidance of the use of a SiC grinding wheel in the first place. Therefore, an MMC can be formed with just Al_2O_3 using thermodynamic calculations for standard D2, as Al_2O_3 acts inert. This could increase the recyclability of D2 grinding swarf.

Acknowledgements

This research was done in the framework of the project “EnerGieeffizIENTe Kreislaufwirtschaft kritischer Rohstoffe (GENESIS)”, which is funded by the Bundesministerium für Wirtschaft und Energie (BMWE) according to a decision of the German Federal Parliament. The funding is highly acknowledged. GENESIS is a joint project between the Ruhr-Universität Bochum, the Bergische Universität Wuppertal, the RWTH Aachen and the Forschungszentrum Jülich as scientific institutions, the German companies WILLO SE, August Berghaus GmbH, Berger Gruppe as end users and Glamatronic, OWL, and Dr. Fritsch Sondermaschinen GmbH as equipment manufacturers. Experimental support of Ralf Steinert (FAST/SPS) and Franco De Angelis (FAST/SPS) is highly acknowledged. Thank you to Prof. Arne Röttger and Dr. Sebastian Jäger of BUW for providing the D2 swarf. Thank you to Dr. Doris Sebold at Forschungszentrum Jülich for performing SEM analysis of the D2 swarf. Thank you to Michelle Treppmann of RUB for conducting tunneling rig experiments.

Open Access funding enabled and organized by Projekt DEAL.

Conflict of Interest

The authors declare no conflict of interest.

Data Availability Statement

The data that support the findings of this study are available from the corresponding author upon reasonable request.

Keywords

direct recycling, field-assisted sintering, grinding swarf, metal matrix composite, tool steel

Received: June 18, 2025
Revised: September 11, 2025
Published online: October 3, 2025

- [1] H. Puga, J. Barbosa, D. Soares, F. Silva, S. Ribeiro, *J. Mater. Process. Technol.* **2009**, 209, 5195.
- [2] Modern Casting Staff, *Mod. Cast.* **2021**, 111, 28.
- [3] P. Li, X. Li, F. Li, *J. Clean. Prod.* **2020**, 266, 121732.
- [4] C.-M. Lee, Y.-H. Choi, J.-H. Ha, W.-S. Woo, *Int. J. Precis. Eng. Manuf.-Green Technol.* **2017**, 4, 457.
- [5] S. Ramanath, T. C. Ramaraj, M. C. Shaw, *CIRP Ann.* **1987**, 36, 245.
- [6] J. Kopac, P. Krajnik, *J. Mater. Process. Technol.* **2006**, 175, 278.
- [7] J. Ni, Y. Yang, C. Wu, *J. Clean. Prod.* **2019**, 212, 593.
- [8] H. Fu, M. A. Matthews, L. S. Warner, *Waste Manag.* **1998**, 18, 321.
- [9] M. Grosso, A. Motta, L. Rigamonti, *Waste Manag.* **2010**, 30, 1238.
- [10] H. Fu, M. A. Matthews, *J. Hazard. Mater.* **1999**, 67, 197.
- [11] H. Fu, M. A. Matthews, *Sep. Sci. Technol.* **1999**, 34, 1411.
- [12] P. Nuss, E. M. Harper, N. T. Nassar, B. K. Reck, T. E. Graedel, *Environ. Sci. Technol.* **2014**, 48, 4171.
- [13] K. Singh, R. K. Khatirkar, S. G. Sapate, *Wear* **2015**, 328–329, 206.
- [14] F. Großwendt, V. Bürk, B. Kopanka, S. Jäger, S. Pollak, L. Leich, A. Röttger, M. Petermann, S. Weber, *J. Clean. Prod.* **2023**, 392, 136329.
- [15] A. N. Lovik, C. Hagelüken, P. Wäger, *Sustain. Mater. Technol.* **2018**, 15, 9.
- [16] X. Hu, C. Wang, M. K. Lim, S. C. L. Koh, *J. Clean. Prod.* **2020**, 243, 118576.
- [17] A. Nygaard, *Circ. Econ. Sustain.* **2023**, 3, 1099.
- [18] W. Hagedorn, S. Jäger, L. Wiczorek, P. Kronenberg, K. Greiff, S. Weber, A. Roettger, *J. Clean. Prod.* **2022**, 377, 134439.
- [19] G. F. Bocchini, *Powder Metall.* **1983**, 26, 101.
- [20] J. Teubler, S. Weber, P. Suski, I. Peschke, C. Liedtke, *J. Clean. Prod.* **2019**, 237, 117775.
- [21] N. G. Razumov, D. V. Masaylo, A. O. Silin, E. V. Borisov, N. E. Ozerskoy, I. S. Goncharov, A. A. Popovich, *J. Manuf. Process.* **2021**, 64, 1070.
- [22] A. Canakci, T. Varol, *J. Clean. Prod.* **2015**, 99, 312.
- [23] S. Jäger, S. Weber, A. Röttger, *Procedia CIRP* **2021**, 104, 893.
- [24] V. Mamedov, *Powder Metall.* **2002**, 45, 322.
- [25] Z. A. Munir, U. Anselmi-Tamburini, M. Ohyanagi, *J. Mater. Sci.* **2006**, 41, 763.
- [26] Y. F. Yang, M. Qian, *Titan. Powder Metall.*, Elsevier, Netherlands **2015**, 219.
- [27] Y. Tomohiro, T. Threrujirapapong, I. Hisashi, K. Katsuyoshi, *Trans. JWRI* **2009**, 38, 37.
- [28] M. Eriksson, Z. Shen, M. Nygren, *Powder Metall.* **2005**, 48, 231.
- [29] M. Zadra, F. Casari, L. Girardini, A. Molinari, *Powder Metall.* **2008**, 51, 59.
- [30] G. Xie, O. Ohashi, K. Chiba, N. Yamaguchi, M. Song, K. Furuya, T. Noda, *Mater. Sci. Eng. A* **2003**, 359, 384.
- [31] S. W. Wang, L. D. Chen, Y. S. Kang, M. Niino, T. Hirai, *Mater. Res. Bull.* **2000**, 35, 619.
- [32] T. Jin, D. J. Stephenson, *Proc. Inst. Mech. Eng. Part B J. Eng. Manuf.* **2006**, 220, 615.
- [33] K. K. Rane, P. P. Date, *J. Sustain. Metall.* **2017**, 3, 251.
- [34] D. K. Kim, H.-R. Pak, K. Okazaki, *Mater. Sci. Eng. A* **1988**, 104, 191.
- [35] C. Musa, R. Licheri, A. M. Locci, R. Orrù, G. Cao, M. A. Rodriguez, L. Jaworska, *J. Clean. Prod.* **2009**, 17, 877.
- [36] F. Maccari, T. P. Mishra, M. Keszler, T. Braun, E. Adabifiroozjaei, I. Radulov, T. Jiang, E. Bruder, O. Guillon, L. Molina-Luna, M. Bram, O. Gutfleisch, *Adv. Eng. Mater.* **2023**, 25, 2300252.
- [37] H. Torkamani, Sh. Raygan, J. Rassizadehghani, *Mater. Des.* **1980-2015** **2014**, 54, 1049.
- [38] G. Linnert, *Welding Metallurgy*, American Welding Society **1994**.
- [39] B. Smoljan, *J. Mech. Eng.* **2010**, 56, 115.
- [40] H. Larsson, *Calphad* **2014**, 47, 1.
- [41] Thermo-Calc Software **2021**.
- [42] L. Brackmann, A. Röttger, M. Treppmann, S. Weber, *Tunn. Undergr. Space Technol.* **2023**, 137, 105151.
- [43] L. Brackmann, D. Wingender, S. Weber, D. Balzani, A. Röttger, *Fatigue Fract. Eng. Mater. Struct.* **2023**, 46, 3872.
- [44] M. Keszler, F. Grosswendt, A. Assmann, A. Röttger, S. Weber, O. Guillon, M. Bram, *Proc. 2024 Powder Metall. World Congr. Exhib.*, Japan Society Of Powder And Powder Metallurgy, Yokohama **2024**, 766.
- [45] M. F. C. Moscoso, F. D. Ramos, C. R. de Lima Lessa, P. H. C. P. Cunha, J. C. Toniolo, G. V. B. Lemos, *J. Mater. Eng. Perform.* **2020**, 29, 7929.
- [46] H. Eifert, G. Veltl, J. Rickel, J. Eckbrecht, A. Schulz, *Pulvermetall. Von Schleifschlämmen Schleifschlamm Als Mögliche Neue Quelle Für Met.* **1996**, 50, 388.